Photometric Capabilities and Scientific Applications of the Meshtitsa Private Observatory

Nikola Antonov^{1,2}

¹ Institute for Advanced Physical Studies, 111 Tsarigradsko Shose Blvd., Sofia, Bulgaria ² Department of Astronomy, Faculty of Physics, Sofia University, 5 James Bourchier Blvd. nikola.antonov@iaps.institute

(Submitted on 08.07.2025; Accepted on 10.10.2025)

Abstract. This paper presents the Meshtitsa Observatory³ - a small-aperture technical platform for high-precision photometric astronomical observations. Located near Pernik, Bulgaria, it is a privately operated roll-off-roof facility equipped with a 0.25-m telescope, CMOS camera, and photometric filters. All operations are remotely managed using a Debian-based INDIGO server infrastructure. The observatory has successfully captured light curves of cataclysmic stars, stellar flares, and transit events of hot Jupiter-type exoplanets with sufficient photometric precision for scientific analysis. These results demonstrate the viability of small-aperture observatories.

Key words: observatory instrumentation, photometry, cataclysmic variable stars, stellar flares, exoplanet transits, citizen science cooperation

Introduction

Within professional optical astronomy, telescopes are commonly sorted by aperture into small ($D \leq 2\,\mathrm{m}$), medium (2–5 m) and large (6–12 m) categories [National Research Council, 2015, p. 26-27]. In the non-professional realm, the threshold shifts downward; the NASA's Exoplanet Watch program, for example, designates any instrument with $D \leq 1\,\mathrm{m}$ as 'small' and shows that telescopes as modest as 0.15–0.25 m routinely supply transit ephemerides and high-cadence light curves of variable targets [Zellem et al., 2020]. Because they are affordable, easily automated, and rapidly re-tasked, small telescopes remain indispensable for tracking swiftly evolving phenomena, ranging from near-Earth asteroids and cataclysmic variable stars to shallow exoplanet transits, and they often provide the first layer of discovery and follow-up, leaving larger telescopes free for deep imaging and high-resolution spectroscopy.

Cataclysmic variables (CVs) are a group of stars that show sudden and unpredictable changes in brightness. Nowadays, it is well known that their high-amplitude outbursts are due to an increased accretion rate onto the disk formed around the more massive companion of a close binary system, comprised of a white dwarf and a late-type main-sequence star. Their erratic behavior has attracted both professional and non-professional astronomers. Even small telescopes make them visible, and hundreds more can be monitored using modern CCD/CMOS cameras. The field is especially open to community contributions, as professionals cannot monitor all known objects.

The study of distant planets has also become a field of activity for both professional and citizen scientists. Several indirect methods for exoplanet research and discovery have been utilized, most notably the transit method, which is available for small-aperture ground-based observations - a telescope with an aperture of 0.25 m can achieve accurate enough results to obtain a good model fit, e.g. [Fowler et al., 2021].

³ https://astro.iaps.institute

Stellar flares are high-energy events on stellar surfaces, triggered by the reconnection of magnetic field lines. They are believed to occur in the upper atmosphere of all main-sequence stars that possess a convective layer and are driven by similar physical processes. In the Sun, flares arise in regions of enhanced magnetic activity, whereas in M-dwarf stars, these events seem to occur across the whole stellar surface [Benz and Güdel, 2010].

In this study, we present results from observations of CV stars - a newly discovered dwarf-nova superhumps during superoutburst, exoplanet transit, and stellar flares of an M-dwarf star conducted at the Meshtitsa Observatory, indicating sufficient photometric precision of small astronomical telescopes, operated entirely remotely and in an automated manner.

1 System Configuration

1.1 Telescope

The Meshtitsa Observatory is equipped with a Sky-Watcher Telescope N 250/1200 PDS Explorer BD OTA^4 , shown in Fig. 1. The optical parameters of the system are shown in Table 1.

| Table 1. Sky-Watche | r Telescope N | 250/1200 | PDS E | xplorer | Parameters |
|---------------------|---------------|----------|-------|---------|------------|
|---------------------|---------------|----------|-------|---------|------------|

| Parameter | Value |
|---------------------|-------------------------------|
| Optical design | Parabolic Newtonian reflector |
| Aperture (mm) | 250 |
| Focal length (mm) | 1 200 |
| Aperture ratio (f/) | 4.8 |
| Tube length (mm) | 1 120 |
| Tube weight (kg) | 14.5 |

Although operating near the limits of its load capacity, the German equatorial mount EQ6-R $\rm Pro^5$ provides reliable object tracking. Automatic guiding is achieved using a TS Optics Guidescope AC $\rm 80/600^6$ with an ASI290MC guiding camera⁷. The guiding process is controlled by the INDIGO software framework, which supports a variety of guiding algorithms to ensure stable tracking and high-quality guiding performance during long exposure sequences. The system is optimized to deliver an average RMSE guiding error below $\rm 0.5''$. The entire system is managed by the $\rm \it INDIGO$ platform and the $\it Ain \it IN-INIGO$

The entire system is managed by the *INDIGO* platform and the *Ain IN-DIGO Imager* running on a Linux operating system, which is also being used at professional observatories⁸. The INDIGO software enables full remote control

⁴ https://skywatcher.com/product/bkp-250-ds/

⁵ https://skywatcher.com/product/eq6r-pro/

https://www.teleskop-express.de/en/telescopes-4/achromatic-refractor-54/ts-optics-guiding-scope-80-600-mm-with-adjustable-tube-rings-8797

⁷ https://www.zwoastro.com/product-category/cameras/

⁸ https://www.indigo-astronomy.org/

and an automated workflow, including pointing, highly detailed task scheduling for exact times, roof opening and closing, and sky-condition monitoring in cooperation with a $CloudWatcher^9$ device (cloud cover monitoring, precipitation, and alarms when unfavorable weather conditions arise). With this integrated software-and-hardware setup, the observatory operates completely autonomously, eliminating the need for constant supervision during observations.



Fig. 1. The telescope at the Meshtitsa Observatory, a $0.25\,\mathrm{m}$ Sky-Watcher Newtonian reflector (f/4.8, focal length $1200\,\mathrm{mm}$) mounted on an EQ6-R Pro German equatorial mount.

1.2 Filters

The telescope at the Meshtitsa Observatory is equipped with a photometric $Baader\ UBVR\ Bessel\ Filter\ Set\ 36\ mm^{10}$.

⁹ https://lunaticoastro.com/aag-cloud-watcher/

https://www.baader-planetarium.com/en/baader-ubvri-bessel-filter-set-photometric.html

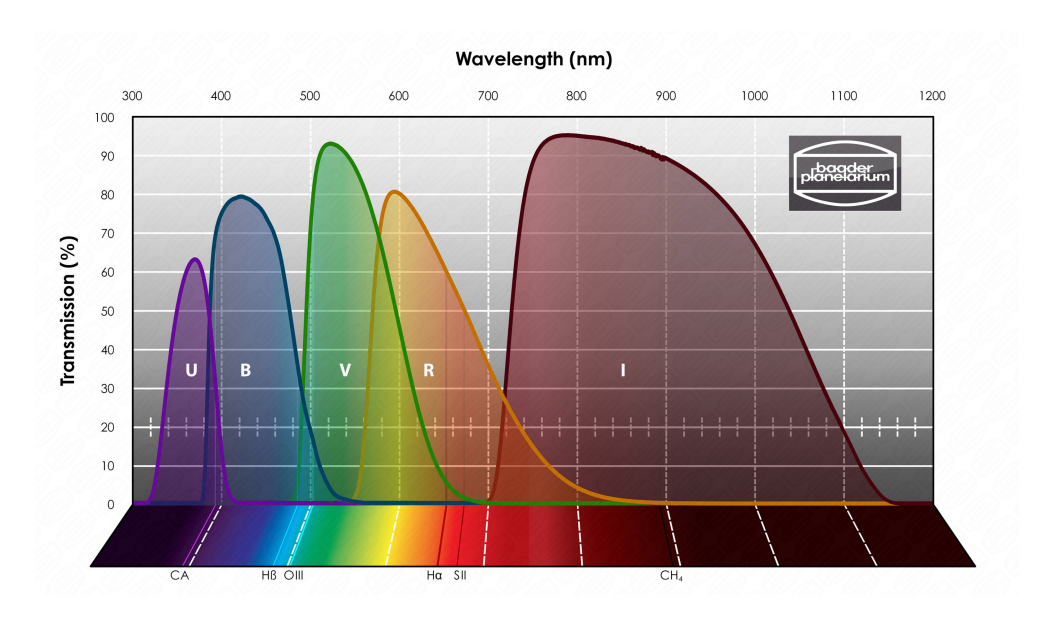


Fig. 2. Spectral profile of Baader Bessel-UBVRI Filters. Image source: https://www.baader-planetarium.com/

Following best practices and the recommendations outlined in the AAVSO Guide to CCD/CMOS Photometry, Chapter 6^{11} , tests were conducted to improve photometric accuracy by imaging standard fields to measure transformation coefficients for each filter. The coefficients shown in Table 2 are derived using the AAVSO Transform Generator 12 .

Table 2. Standard-system transformation coefficients derived for the Meshtitsa telescope

| Coefficient | Value | Error |
|-------------|--------|-------|
| | | |
| T_{ub} | 1.000 | 0.066 |
| T_{u_ub} | 0.096 | 0.070 |
| T_{b_ub} | 0.059 | 0.011 |
| T_{bv} | 1.095 | 0.009 |
| T_{b_bv} | 0.080 | 0.012 |
| T_{br} | 1.144 | 0.013 |
| T_{b_br} | 0.050 | 0.006 |
| T_{v_bv} | -0.008 | 0.015 |
| T_{vr} | 1.255 | 0.033 |
| T_{v-vr} | -0.012 | 0.025 |
| T_{r_vr} | -0.221 | 0.030 |

¹¹ https://www.aavso.org/ccd-camera-photometry-guide

¹² https://www.aavso.org/tg

1.3 Camera

The ASI 533 MM Pro¹³ camera is a high-performance monochrome imaging device well-suited for both artistic astrophotography and scientific research, see Fig. 3. It features a Sony IMX533 back-illuminated CMOS sensor. One of its major advantages is the complete absence of amp glow, which results in exceptionally clean raw images and simplifies the calibration process.



Fig. 3. Camera ASI533 MM Pro CMOS, filter wheel, and automatic focuser mounted on the 0.25-m telescope

The ASI 533 MM Pro also has a dual-stage TEC cooling system that can reduce the sensor temperature by up to 35°C below ambient, effectively minimizing thermal noise during long exposures. The camera parameters are summarized in Table 3.

The sensor quantum efficiency curve (QE), shown in Fig. 4 peaks above 90% in the blue-green part of the spectrum (approximately 450 - 500 nm), making it highly efficient for most photometric work in the B, V, and R bands. ASI 533 MM Pro has limited sensitivity in the U band, with quantum efficiency dropping significantly around 350 - 400 nm. Although U-band photometry can

¹³ https://www.zwoastro.com/product/asi533-pro-series/

Table 3. ASI 533 MM Pro Camera Parameters. Source: https://www.zwoastro.com/product/asi533-pro-series/

| Parameter | Value |
|---|---|
| Sensor | CMOS Chip (Sony IMX533) |
| Light spectrum | U (limited sensitivity) + Visible + NIR |
| Total pixels | 9 MP |
| Resolution WxH | $3~008 \times 3~008~{\rm px}$ |
| Pixel size | $3.76~\mu m$ |
| Bit depth | 14 |
| Full well capacity | 50 000 |
| Max. cooling difference below ambient temperature | $35^{\circ}\mathrm{C}$ |
| Weight | 410 g |

be performed with this camera, it requires considerably longer exposures than in the B- or V-band.

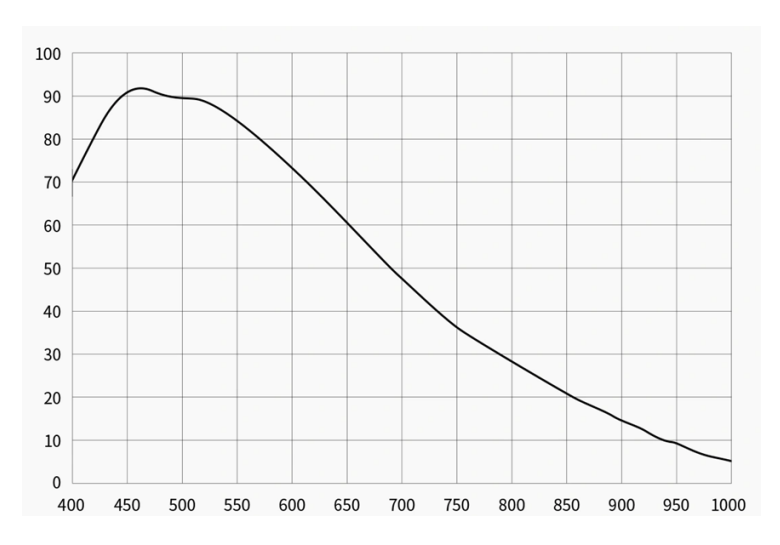


Fig. 4. Quantum Efficiency of ASI533MM Pro CMOS camera according to the manufacturer's website. Image source: https://www.zwoastro.com/product/asi533-pro-series/

A linearity test was conducted under stable observational conditions. The ASI533MM Pro camera was operated at a constant sensor temperature of 0° C, using a steady, uniformly illuminated surface as the light source. A broadband L (luminance) filter was placed in the optical path. Exposure times were varied from 1.0 to 15.0 seconds in steps of 1.0 second, and the camera settings were fixed at Gain = 0 and Offset = 10 to maximize dynamic range. For each exposure, the mean ADU value for the frame was measured.

The resulting data, shown in Fig. 5 demonstrate a well-defined linear response up to approximately 60 000 ADU. Beyond this level, the response be-

gins to flatten as the detector approaches its saturation regime. Although the sensor uses a 14-bit analog-to-digital converter (ADC), its output is internally mapped to a 16-bit format, allowing for digital values up to 65 535. The maximum recorded value in fully saturated pixels is 65 532 ADU. For optimal photometric results, exposures should be adjusted to keep the peak signal below $\sim\!60\,000$ ADU, thereby avoiding non-linear compression near the ADC ceiling.

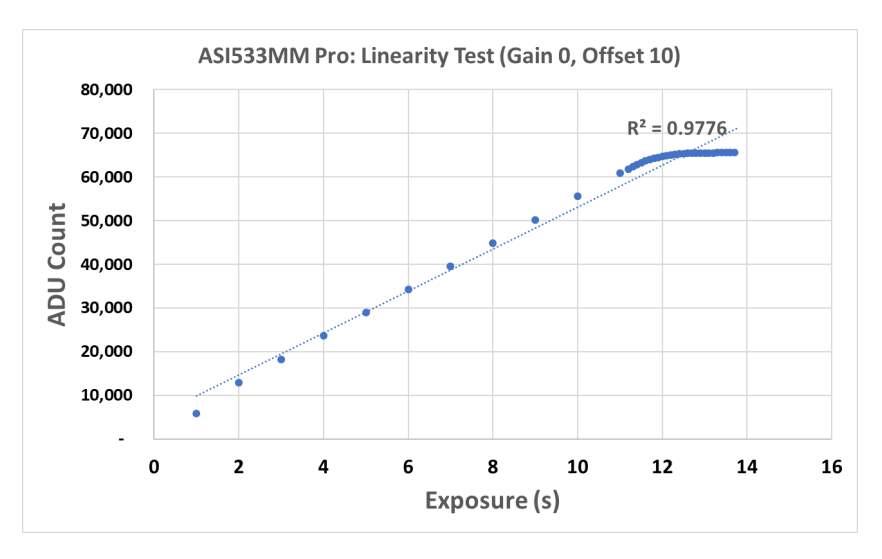


Fig. 5. Linearity test for the ASI533MM camera in Meshtitsa Observatory showing relation between ADU counts and exposure time

1.4 Optical Performance

The Meshtitsa Observatory is located near Pernik, Bulgaria at an altitude of 695 m. The typical seeing conditions are characterized by FWHM between 2.0" and 2.5". Under a clear, moonless night, and with the telescope pointed at an altitude of at least 60° above the horizon, the current optical system achieves a limiting magnitude of ≈ 17.5 in the V band with a 30-second exposure at a signal-to-noise ratio of ≈ 7 , which was estimated by the astrometric software ASTAP¹⁴. Long-term measurements performed over several months with a Lunatico Astronomia $CloudWatcher^{15}$ indicate that the maximum sky darkness at the site reaches $19.7 \, \text{mag/arcsec}^2$.

For a system with 3.76 µm pixel size and 1 200 mm focal length a scale of 0.64'' per pixel is close to oversampling for typical seeing conditions at a given location. At 2×2 binning, the resulting pixel scale is approximately 1.3'' per pixel, which better matches the atmospheric resolution limit. At a focal length

¹⁴ https://www.hnsky.org/astap.htm

¹⁵ https://www.lunaticoastro.com

of 1,200 mm, combined with the sensor size of 11.31 \times 11.31 mm, the system provides a field of view of approximately 0.5° \times 0.5°.

As an example, Fig. 6 shows a stellar field from a 30-second calibrated science image of the NGC 7790 star cluster.

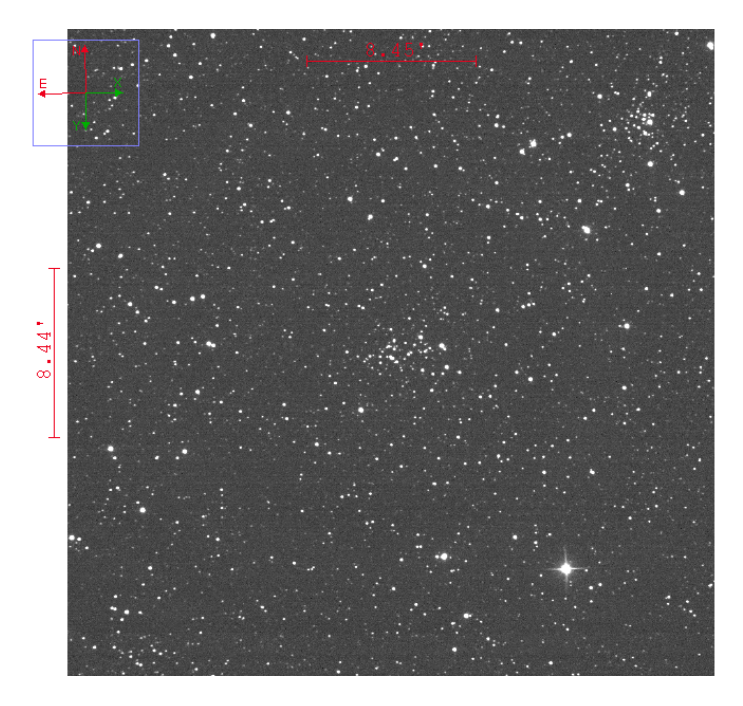


Fig. 6. Single calibrated frame of the stellar field NGC 7790 obtained with the V filter (30s exposure, 2×2 binning, gain 0, offset 10).

1.5 Calibration Strategy

The calibration of the science images followed standard CCD reduction procedures, including the acquisition of bias, dark, and flat-field frames, and was performed using AstroImageJ [Collins et al., 2017, p. 4], as illustrated in Fig. 7.

Bias frames were obtained with the telescope aperture closed, using an exposure time of 0 s. A total of 99 bias frames were acquired and later combined using the median method.

Dark frames were also taken with the telescope aperture closed, matching both the exposure time and the CCD temperature used during the scientific observations. Typically, the camera operated at -20° C, a temperature at which, according to the manufacturer's specifications, the thermal noise of the detector is negligible. If environmental conditions did not allow operation at this temperature, the camera was set to at least -15° C. For each of these

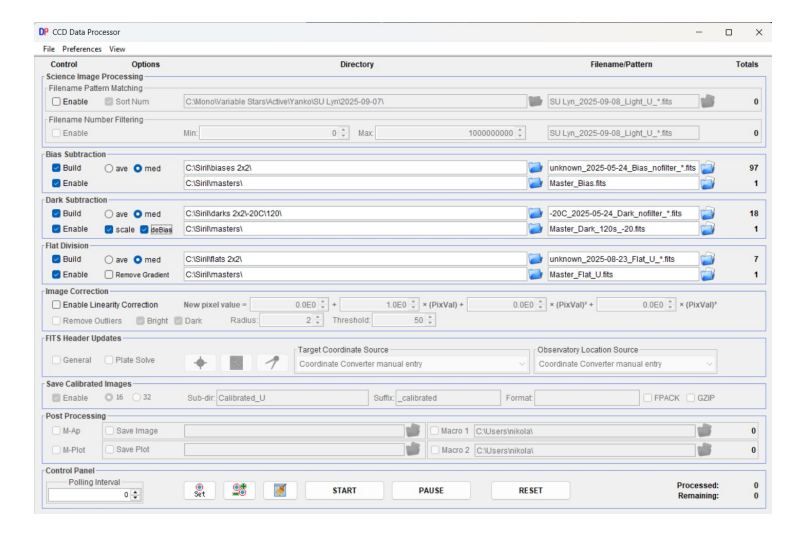


Fig. 7. AstroImageJ Data Processor interface for building master calibration frames and calibration of science images

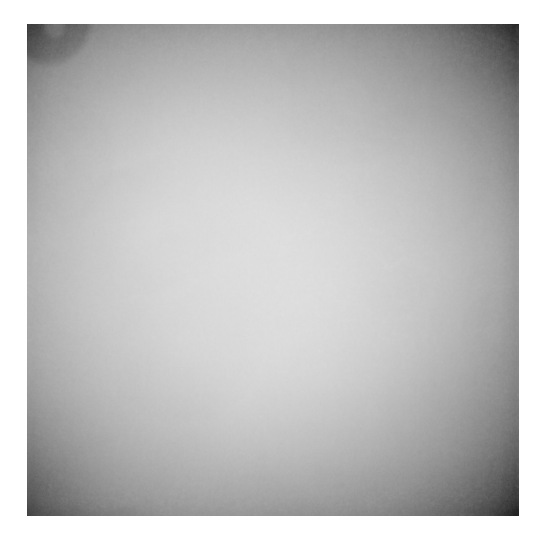


Fig. 8. Master flat field obtained in the V filter, created from the median combination of multiple twilight flats.

operating temperatures, dedicated dark frames were obtained using the same exposure and temperature as those in the observations.

Flat fields, see Fig. 8, were obtained immediately after sunset. The exposure time was adjusted so that the mean pixel value in each frame was maintained at $\sim \! 30\,000\,\mathrm{ADU}$, well within the linear response range of the camera. At least seven flat-field frames were taken for each filter, and all calibration frames were stacked using median combining to remove cosmic rays and residual artifacts.

2 Results

Data from the Meshtitsa Observatory are available through the $AAVSO^{16}$ and are already being used in astronomical research. Exoplanet transit observations have likewise been incorporated into NASA's $Exoplanet\ Watch^{17}$ database. The following section presents several new results that demonstrate the capabilities of small telescopes such as the one at the Meshtitsa Observatory.

2.1 Superhumps of dwarf nova GOTO065054+593624

The dwarf nova GOTO065054+593624 (GOTO0650) was discovered on 4 October 2024 [Killestein et al., 2024], by the *GOTO* all-sky survey¹⁸ and quickly identified by volunteers from the *Kilonova Seekers*¹⁹. Their rapid classification allowed immediate follow-up, revealing a WZ Sge type cataclysmic star with an 8.5-magnitude outburst [Killestein, T. L. et al., 2025]. The Meshtitsa Observatory joined the follow-up campaign and conducted observations over 26 nights, spanning 98 hours, across a two-month period, making it one of the sites that detected the first superhumps of the star during its outburst.

Table 4. Photometric observations of GOTO0650 with superhump period determination

| $\begin{array}{c} \textbf{Obs. Start} \\ \textbf{UTC} \end{array}$ | $\begin{array}{c} { m Obs.} \ { m End} \\ { m UTC} \end{array}$ | | Mean Mag. V | | _ | Period |
|---|--|--------------------------|--|--|--|--|
| 10/20/2024 19:45 10/22/2024 19:18 10/23/2024 19:48 10/25/2024 19:38 10/26/2024 19:28 10/27/2024 19:49 | 10/23/2024 2:54 10/24/2024 2:42 10/26/2024 2:56 10/27/2024 2:22 | 7.6 6.9 7.3 6.9 | 14.220 14.275 14.352 14.534 14.639 14.744 | 0.011 0.016 0.013 0.015 0.015 0.015 | 0.055 0.034 0.032 0.030 0.025 0.022 | 0.06332 0.06293 0.06382 0.06327 0.06196 0.06334 |

Among all observations, superhumps were identified in a total of 6 instances. The observations listed in Table 4, were processed using AstroImageJ (AIJ). The periodogram at Fig. 9 reveals the first detected superhumps for the GOTO0650, visible as periodic brightness modulation with an amplitude of 0.06 (M). Using the Generalized Lomb–Scargle [Zechmeister and Kürster, 2009], the superhump period was determined to be $\approx 91 \pm 1$ min.

The superhump period is crucial for determining the mass ratio of the system's components [Kato and Osaki, 2013]. This is done through the *superhump* period excess,

$$\epsilon = \frac{P_{\rm sh}}{P_{\rm orb}} - 1 \tag{1}$$

¹⁶ https://www.aavso.org/

¹⁷ https://exoplanets.nasa.gov/exoplanet-watch/about-exoplanet-watch/overview/

¹⁸ https://goto-observatory.org/

¹⁹ https://www.zooniverse.org/projects/tkillestein/kilonova-seekers

where $P_{\rm sh}$ is the measured superhump period and $P_{\rm orb}$ is the orbital period of the binary.

Typical superhump period excesses in WZ Sge systems range from 0.8% to 1.5%. Assuming GOTO0650 follows this trend, the orbital period can be tentatively constrained to lie in the 88–90 minute range, e.g. [Killestein, T. L. et al., 2025]. However, applying this relation requires an independent measurement of the orbital period $P_{\rm orb}$, typically obtained through radial velocity studies.

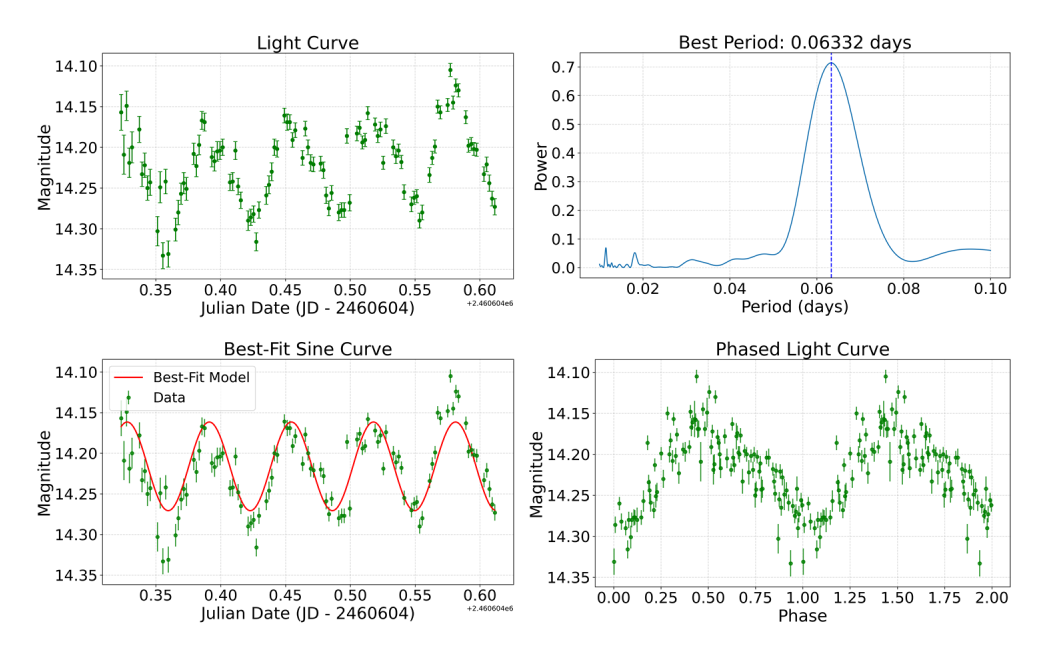


Fig. 9. Periodogram and V-band light curve from the first observing night on Oct 20, 2024 on which superhumps of GOTO0650 were detected. The period derived with the Generalized Lomb–Scargle algorithm was used to compute the best-fitting sinusoid over the original photometric data

2.2 Transit of exoplanet TOI-2109b on March 22, 2024

TOI-2109b is an ultrahot Jupiter-like exoplanet discovered in 2021 by NASA's Transiting Exoplanet Survey Satellite²⁰ (TESS). The planet orbits an F-type star located about 855 light years away. TOI-2109b possesses a mass of approximately 5.02 Jupiter masses and a radius about 1.35 Jupiter radii. Observations of newly discovered exoplanets are particularly valuable, as their ephemerides are still being refined.

A transit of TOI-2109b was observed from Meshtitsa Observatory on March 22, 2024. The observation was conducted using a photometric V filter with an

²⁰ https://tess.mit.edu/

exposure time of 60 seconds per frame. Over approximately 4 hours, a total of 215 frames were captured. Both the photometric measurements and the transit model fit, shown in Fig. 10, were derived using AIJ's built-in differential photometry and fitting tools.

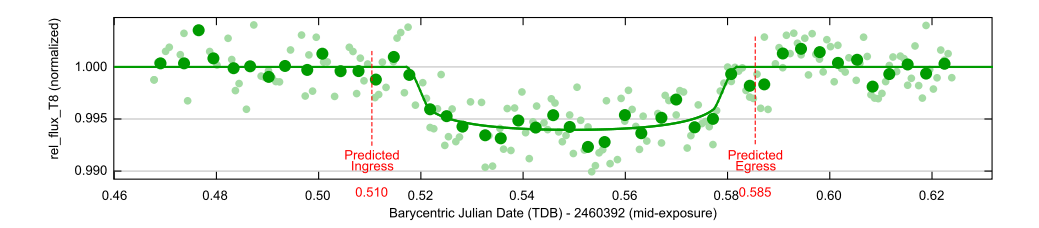


Fig. 10. Relative flux light curve of TOI-2109b based on 215 V-band exposures taken on 22 March 2024. The data points represent the differential photometry of the target star using nearby comparison stars. The smooth model curve shows the best-fit transit profile calculated within AstroImageJ, based on the observed flux decrease during the planetary transit. The characteristic U-shape reflects the partial occultation of the stellar disk by the orbiting planet.

The transit light curve of TOI-2109b obtained on 22 March 2024 was modeled using the fitting tools in AstroImageJ. The best-fit parameters are consistent with the published ephemerides, e.g. [Wong et al., 2021]. The fitted planet-to-star radius ratio is $(R_p/R_{\star})^2=0.00511$, corresponding to a transit depth of 6.0 ppt. The total transit duration was measured as $t_{14}=0.0646\,\mathrm{d}$ (1^h33^m01^s). Assuming the stellar radius $R_{\star}=1.447\,R_{\odot}$, this corresponds to a planetary radius of $R_p=1.01\,R_{\mathrm{Jup}}$. The fit yields a nearly central transit geometry with an inclination of $i\approx 90^{\circ}$ and an impact angle close to zero. The quality of the fit is reflected by the statistical indicators: the RMS of the residuals is 0.00207 in normalized flux ($\sim 2.1\,\mathrm{ppt}$), and the reduced chi-square is $\chi^2/\mathrm{dof}=1.07$.

2.3 Flares of AD Leo captured between 16 January and 2 May 2025

AD Leo is a dM3.5e star, only about 5 pc from the Sun. Statistical analyses indicate that it produces energetic flares at a moderate rate and ranks among the most thoroughly studied flare stars in the solar neighborhood, e.g. [Pettersen and Coleman, 1981].

Table 5 lists 16 B-band flares of AD Leo observed with a 30-s cadence between 16 January and 2 May 2025. Energies were calculated by applying the standard time integration of the luminosity, widely formalized by flare-energy studies, e.g. [Hunt-Walker et al., 2012]. The software used in this study is a custom in-house program developed specifically for this project. At present, it is not publicly released. However, the algorithms and analysis steps are fully described [Hunt-Walker et al., 2012], allowing others to reproduce the results or implement similar procedures independently.

Table 5. Flares of AD Leo captured between 16 January and 2 May 2025 in B band (Johnson B filter) with a 20-seconds cadence

| | Flare Start | Flare End | Dur. | Peak | Peak | δ | Energy in B |
|-----------------|---------------|---------------|-------|---------------|-------|----------|-------------|
| No. | JD | JD | (min) | JD | Mag. | Mag. | (erg) |
| | | | | | | | |
| 1 | | 2460695.42996 | 45 | 2460695.40336 | | 0.51 | 1.90e + 32 |
| 2 | 2460710.32434 | 2460710.33953 | 22 | 2460710.32990 | 10.66 | 0.18 | 2.48e + 31 |
| 3 | 2460712.39542 | 2460712.42106 | 37 | 2460712.40529 | 10.69 | 0.15 | 1.60e + 31 |
| 4 | 2460721.37398 | 2460721.38063 | 10 | 2460721.37651 | 10.78 | 0.06 | 1.74e + 30 |
| 5 | 2460727.39928 | 2460727.41245 | 19 | 2460727.40507 | 10.04 | 0.81 | 7.00e + 31 |
| 6 | 2460727.41513 | 2460727.42673 | 17 | 2460727.41738 | 10.69 | 0.16 | 1.45e + 31 |
| 7 | 2460729.45763 | 2460729.46819 | 15 | 2460729.46021 | 10.74 | 0.11 | 3.47e + 31 |
| 8 | 2460729.51584 | 2460729.52411 | 12 | 2460729.51942 | 10.77 | 0.08 | 3.38e + 30 |
| 9 | 2460732.31972 | 2460732.38421 | 93 | 2460732.32789 | 10.11 | 0.74 | 1.06e + 33 |
| 10 | 2460732.38772 | 2460732.39952 | 17 | 2460732.39038 | 10.10 | 0.75 | 3.02e + 32 |
| 11 | 2460739.31536 | 2460739.33539 | 29 | 2460739.32174 | 10.46 | 0.39 | 2.28e + 32 |
| 12 | 2460739.33812 | 2460739.38395 | 66 | 2460739.34096 | 10.04 | 0.81 | 2.46e + 32 |
| 13 | 2460739.46924 | 2460739.48108 | 17 | 2460739.47281 | 10.58 | 0.27 | 3.21e + 31 |
| 14 | 2460756.27626 | 2460756.30324 | 39 | 2460756.27891 | 10.33 | 0.51 | 1.90e + 32 |
| $\overline{15}$ | | 2460773.28845 | 14 | 2460773.28205 | | 0.09 | 2.63e + 31 |
| 16 | | 2460773.32446 | 11 | 2460773.31929 | | 0.08 | 1.47e + 31 |

Representative AD Leo light curves in Fig. 11 display the classic fast-rise-exponential-decay (FRED) flare profiles.

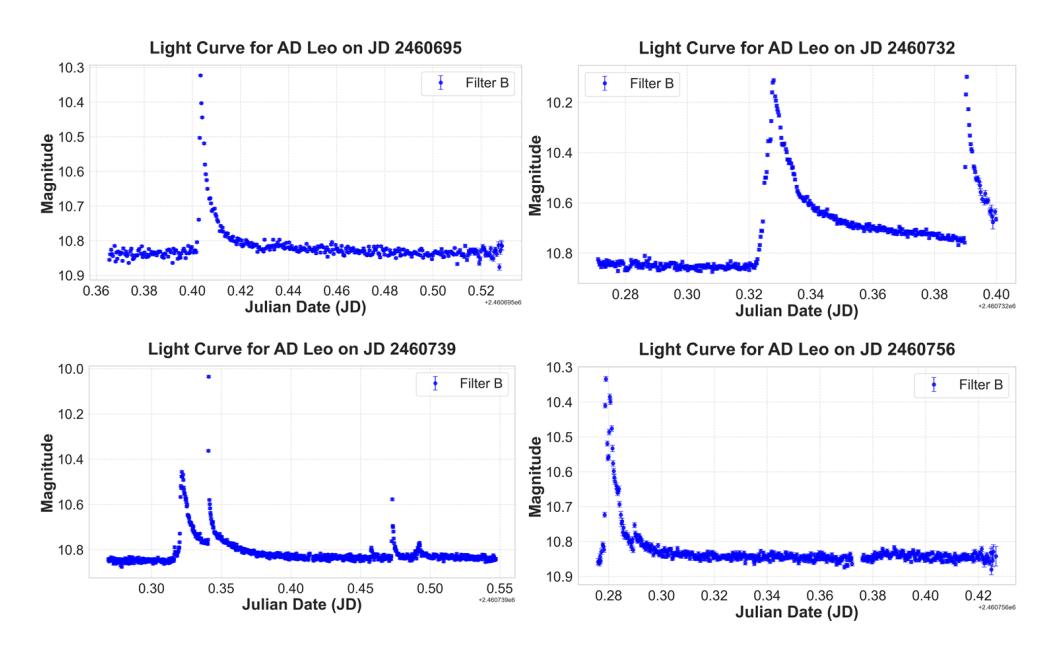


Fig. 11. Light curves of several of the most characteristic AD Leo flares obtained at Meshtitsa Observatory in the B filter with a 20-second exposure cadence

AD Leo is among the most extensively studied flare stars in the solar neighborhood. Previous works have established its high flare rate and energy output, providing a benchmark for statistical analyses. For example, [Hunt-Walker et al., 2012] derived flare-frequency distributions in the optical and confirmed that AD Leo flares follow a canonical power-law, spanning energies from 10^{30} to 10^{34} erg. Our cumulative flare-frequency distribution in the B band (Fig. 12) is consistent with these earlier studies, with the derived slope over the 10^{31} – 10^{32} erg range. This confirms that the energies measured at Meshtitsa Observatory reproduce the well-known flare statistics of AD Leo and demonstrate the reliability of small-aperture telescopes in flare monitoring.

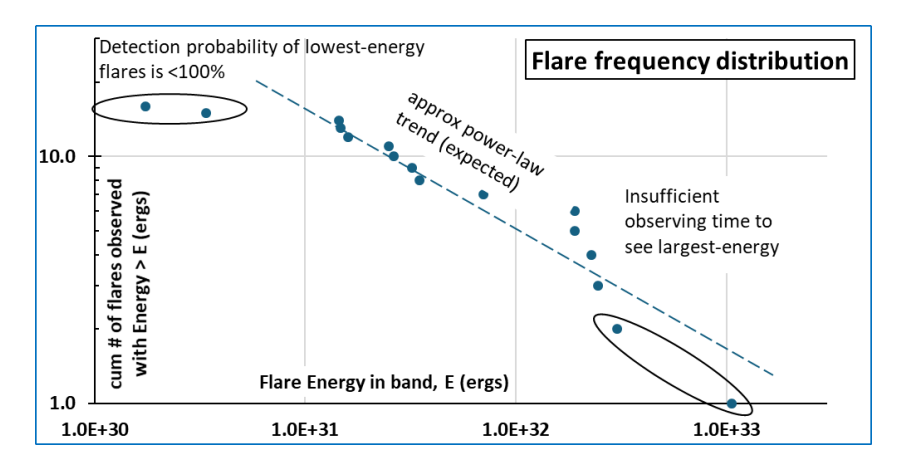


Fig. 12. AD Leo cumulative flare-frequency distribution in the *B* band, derived from 16 flares detected at the Meshtitsa Observatory. Despite the limited statistics (only 16 events), the expected negative linear trend is visible, although the extremes of the distribution show insufficient sampling at the highest and lowest energies.

Conclusion

In this study, selected first results from observations conducted with the remote Meshtitsa Observatory were presented:

- V-band monitoring during the outburst of the nova GOTO065054 revealed the onset of superhumps and yielded a period of 91 ± 1 min, thereby providing an early constraint on the binary mass ratio.
- A transit observation of TOI-2109b revealed a duration of 0.0646 d with a depth of 6.0 ppt, aligning with predicted values, and yielded key statistics on which the planetary radius estimate rests.
- Several *B*-band flares on *AD Leo* were presented. A cumulative flare-frequency distribution was derived, following the canonical power law over 10^{31} – 10^{32} erg.

These results show that observations from small, non-professional observatories achieve sufficient precision for use in professional studies. Their capacity for frequent, targeted monitoring makes them an indispensable part of global astronomical networks, especially for tracking dynamic or unpredictable objects that larger surveys may miss. Beyond the individual results, this work affirms the strategic role of citizen-science observatories in modern time-domain astronomy. Currently, Meshtitsa Observatory continues to conduct regular observations and participate in international campaigns.

Acknowledgment

The author gratefully acknowledges the anonymous reviewers for their thoughtful critiques and recommendations, which helped refine the article. The equipment for the Meshtitsa Observatory was provided through donations from Scorpion Shipping Ltd.²¹ and the Institute for Advanced Physical Studies, Sofia, 111 Tsarigradsko Shose Blvd²². Sincere gratitude is extended to Sean Curry, Bob Buchheim, Gary Hawkins, and Thomas Smith for their assistance with the FFD analysis of AD Leo and for providing the custom Python-based software *PhotoStats*, which was instrumental in performing the flare energy calculations presented in this work.

References

Benz, A. O. and Güdel, M. (2010). Physical processes in magnetically driven flares on the sun, stars, and young stellar objects. Annual Review of Astronomy and Astrophysics, 48(1):241-287.

Collins, K. A., Kielkopf, J. F., Stassun, K. G., and Hessman, F. V. (2017). Astroimagej: Image processing and photometric extraction for ultra-precise astronomical light curves. The Astronomical Journal, 153(2):77.

Fowler, M. J. F., Sienkiewicz, F. F., Zellem, R. T., and Dussault, M. E. (2021). Observing exoplanets with the MicroObservatory: 43 new transit light curves of the hot Jupiter

HAT-P-32b. Journal of the British Astronomical Association, 131:359–368. Hunt-Walker, N. M., Hilton, E. J., Kowalski, A. F., Hawley, S. L., and Matthews, J. M. (2012). Most observations of the flare star ad leo. Publications of the Astronomical Society of the Pacific, 124(916):545.

Kato, T. and Osaki, Y. (2013). New method of estimating binary's mass ratios by using

superhumps. Publications of the Astronomical Society of Japan, 65(6):115.

Killestein, T., Kelsey, L., Ramsay, G., Kennedy, M. R., Kumar, A., Wickens, E., Ackley, K., Dyer, M. J., et al. (2024). GOTO065054.49+593624.51: Discovery of a bright optical galactic transient. The Astronomer's Telegram, 16842.

Killestein, T. L., Ramsay, G., Kennedy, M., Kelsey, L., Steeghs, D., Littlefair, S., Godson, B. L., Lander, M., Wenrich, B. W., Wickens, E.

estein, T. L., Ramsay, G., Kennedy, M., Kelsey, L., Steeghs, D., Littlefair, S., Godson, B., Lyman, J., Pursiainen, M., Warwick, B., Krawczyk, C., Nuttall, L. K., Wickens, E., Alexandrov, S. D., da Silva, C. M., Leadbeater, R., Ackley, K., Dyer, M. J., Jiménez-Ibarra, F., Ulaczyk, K., Galloway, D. K., Dhillon, V. S., O'Brien, P., Noysena, K., Kotak, R., Breton, R. P., Pallé, E., Pollacco, D., Kumar, A., O'Neill, D., Butterley, T., Wilson, R., Mattila, S., Sahu, A., Starling, R., Wang, C. Y., Liu, Q., Li, A., Dai, Z., Feng, H., Yuan, W., Billington, R., Bull, A. G., Gaudenzi, S., Gonano, V., Krawczyk, H., Mazzucato, M. T., Pasqua, A., da Silva Campos, J. A., Torres-Guerrero, M., Antonov, N. N., Bean, S. J., Boeneker, E. T., Brincat, S. M., Darlington, G. S., Dubois, F., Hambsch, F., J., Messier, D., Oksanen, A., Povner, G., Romanov, F. D., Sharn, I. D., Hambsch, F. -J., Messier, D., Oksanen, A., Poyner, G., Romanov, F. D., Sharp, I. D., Tordai, T., Vanmunster, T., and Wenzel, K. (2025). Goto065054+593624: An 8.5 mag amplitude dwarf nova identified in real time via kilonova seekers. AA, 699:A8.

²² https://iaps.institute

 $^{^{21}}$ https://scorpion-shipping.net

National Research Council (2015). Optimizing the U.S. Ground-Based Optical and Infrared Astronomy System. The National Academies Press, Washington, DC.

Pettersen, B. R. and Coleman, L. A. (1981). Chromospheric lines in red dwarf flare stars. i. ad leo and gx and. *The Astrophysical Journal*, 251:571–582.

Wong, I., Shporer, A., Zhou, G., Kitzmann, D., Komacek, T. D., Tan, X., Tronsgaard, R., Buchhave, L. A., Vissapragada, S., Greklek-McKeon, M., Rodriguez, J. E., Ahlers, J. P., Quinn, S. N., Furlan, E., Howell, S. B., Bieryla, A., Heng, K., Knutson, H. A., Collins, K. A., McLeod, K. K., Berlind, P., Brown, P., Calkins, M. L., de Leon, J. P., Esparza-Borges, E., Esquerdo, G. A., Fukui, A., Gan, T., Girardin, E., Gnilka, C. L., Ikoma, M., Jensen, E. L. N., Kielkopf, J., Kodama, T., Kurita, S., Lester, K. V., Lewin, P., Marino, G., Murgas, F., Narita, N., Pallé, E., Schwarz, R. P., Stassun, K. G., Tamura, M., Watanabe, N., Benneke, B., Ricker, G. R., Latham, D. W., Vanderspek, R., Seager, S., Winn, J. N., Louking, J. M., Caldwell, D. A., Fong, W., Huang, G. Y., Mireles, L. S., Winn, J. N., Jenkins, J. M., Caldwell, D. A., Fong, W., Huang, C. X., Mireles, I., Schlieder, J. E., Shiao, B., and Noel Villaseñor, J. (2021). TOI-2109: An Ultrahot Gas Giant on a 16 hr Orbit. AJ, 162(6):256.

Zechmeister, M. and Kürster, M. (2009). The generalised Lomb-Scargle periodogram. A new formalism for the floating-mean and Keplerian periodograms. A&A, 496(2):577-584.

Zellem, R. T., Pearson, K. A., Blaser, E., Fowler, M., Ciardi, D. R., Biferno, A., Massey, B., Marchis, F., Baer, R., Ball, C., Chasin, M., Conley, M., Dixon, S., Fletcher, E., Hernandez, S., Nair, S., Perian, Q., Sienkiewicz, F., Tock, K., Vijayakumar, V., Swain, M. R., Roudier, G. M., Bryden, G., Conti, D. M., Hill, D. H., Hergenrother, C. W., Dussault, M., Kane, S. R., Fitzgerald, M., Boyce, P., Peticolas, L., Gee, W., Cominsky, L., Zimmerman-Brachman, R., Smith, D., Creech-Eakman, M. J., Engelke, J., Iturralde, A.,
D. Leynovic, N. Leyton, B., Arbeute, E., Kuchper, M., and Malyzebe, A. Dragomir, D., Jovanovic, N., Lawton, B., Arbouch, E., Kuchner, M., and Malvache, A. (2020). Utilizing small telescopes operated by citizen scientists for transiting exoplanet follow-up. Publications of the Astronomical Society of the Pacific, 132(1011):054401.